THE JOURNAL OF BIOLOGICAL CHEMISTRY VOL. 291, NO. 8, pp. 3694–3704, February 19, 2016
© 2016 by The American Society for Biochemistry and Molecular Biology, Inc. Published in the U.S.A.

The Structural and Functional Characterization of Mammalian ADP-dependent Glucokinase*

Received for publication, July 21, 2015, and in revised form, October 22, 2015 Published, JBC Papers in Press, November 10, 2015, DOI 10.1074/jbc.M115.679902

Jan P. Richter‡, Alexander K. Goroncy‡, Ron S. Ronimus§1, and Andrew J. Sutherland-Smith‡2

From the ‡Institute of Fundamental Sciences, Massey University, Palmerston North 4410, New Zealand and §AgResearch Limited, Palmerston North 4442, New Zealand

The enzyme-catalyzed phosphorylation of glucose to glucose-6-phosphate is a reaction central to the metabolism of all life. ADP-dependent glucokinase (ADPGK) catalyzes glucose-6-phosphate production, utilizing ADP as a phosphoryl donor in contrast to the more well characterized ATP-requiring hexokinases. ADPGK is found in Archaea and metazoa; in Archaea, ADPGK participates in a glycolytic role, but a function in most eukaryotic cell types remains unknown. We have determined structures of the eukaryotic ADPGK revealing a ribokinase-like tertiary fold similar to archaeal orthologues but with significant differences in some secondary structural elements. Both the unliganded and the AMP-bound ADPGK structures are in the "open" conformation. The structures reveal the presence of a disulfide bond between conserved cysteines that is positioned at the nucleotide-binding loop of eukaryotic ADPGK. The AMP-bound ADPGK structure defines the nucleotide-binding site with one of the disulfide bond cysteines coordinating the AMP with its main chain atoms, a nucleotide-binding motif that appears unique to eukaryotic ADPGKs. Key amino acids at the active site are structurally conserved between mammalian and archaeal ADPGK, and site-directed mutagenesis has confirmed residues essential for enzymatic activity. ADPGK is substrate inhibited by high glucose concentration and shows high specificity for glucose, with no activity for other sugars, as determined by NMR spectroscopy, including 2-deoxyglucose, the glucose analogue used for tumor detection by positron emission tomography.

Glucose metabolism is central to the biochemistry of all living systems with the enzymatic phosphorylation of glucose playing a key role in cellular energy metabolism by ensuring that this energy-rich substrate is available to the cell. A relatively recently discovered ADP-dependent glucokinase (ADPGK)[3] (EC 2.7.1.147) catalyzes the phosphorylation of D-glucose to glucose-6-phosphate using MgADP as phosphoryl donor in contrast to the more typical ATP-utilizing hexokinases and glucokinases. ADPGK was first identified in Archaea, being involved in a modified Embden-Meyerhof glycolytic pathway (1), in which Archaea can also use an ADP-dependent phosphofructokinase (ADPPFK; EC 2.7.1.146). Bioinformatic analysis led to the identification of ADPGK in metazoa and the subsequent cloning and initial characterization of mammalian ADPGKs (2, 3). Mammalian ADPGKs show modest sequence similarity to archaeal orthologues (~20% amino acid identity). ADPGK is highly expressed in a wide variety of both normal and tumor mammalian tissues (3) and has been found to be localized to the endoplasmic reticulum in T cells (4) consistent with the sequence-based annotation of an N-terminal signal peptide. Furthermore, ADPGK has been identified as a cholesterol binding protein in a proteomics screen (5). Despite the role of archaeal ADPGK in glycolysis, overexpression of ADPGK in H460 and HC116 human tumor cells showed no cell proliferative or glycolytic effects (3). ADPGK knock-out in these cell lines showed no detectable effect on glycolysis or extracellular acidification as assay end points, although O_2 consumption was generally lower for the ADPGK knock-out cells (6). Knock-out of ADPGK had no effect on cell survival under normal growth conditions, but ADPGK is protective for H460 cells under anoxia and reduced glycolysis (hexokinase 2 silencing) stress conditions, but not for HCT116 cells (6). ADPGK activity is associated with T cell receptor signaling, resulting in mitochondrial reactive oxygen species production as activated T cells switch from mitochondrial respiration to a dependence on glycolysis (4). Apart from this role in T cells, a function for ADPGK remains to be defined for most eukaryotic cell types.

The crystal structures of three archaeal ADPGKs have been determined in varying liganded states revealing an overall similarity in topology to the ribokinase superfamily and no homology to hexokinases. Archaeal ADPGK crystal structures have been determined for apo-ADPGK from *Pyrococcus horikoshii* OT3 (PDB code 1L2l) (7) and glucose- and AMP-bound *Pyrococcus furiosus* ADPGK (PDB code 1UA4) (8). *Thermococcus litoralis* ADPGK structures have been determined in the ADP-bound form (PDB code 1GC5) (9) and apo (PDB code 4B8R) and AMP/glucose ternary complexes (PDB code 4B8S) (10). The ADPGK structure contains two α/β domains; the large domain is a Rossmann-type fold of an eight-stranded β-sheet enclosed by eight α-helices, with five helices on one side and three on the other. The substrates glucose and ADP bind in a shallow groove in the large domain that is covered over by the small domain acting as a "lid." The different archaeal ADPGK

* This work was supported by the Royal Society of New Zealand Marsden Fund, New Zealand Synchrotron Group, and Massey University. The authors declare that they have no conflicts of interest with the contents of this article.

[1] To whom correspondence may be addressed: Animal Nutrition and Health, AgResearch Limited, Grasslands Research Centre, Tennent Dr., Private Bag 11008, Palmerston North 4442, New Zealand. Tel.: 6463518036; Fax: 6463518032; E-mail: ron.ronimus@agresearch.co.nz.

[2] To whom correspondence may be addressed: Inst. of Fundamental Sciences, Massey University, Tennent Dr., Palmerston North 4442, New Zealand. Tel.: 6469517701; Fax: 6463557947; E-mail: A.J.Sutherland-Smith@massey.ac.nz.

[3] The abbreviations used are: ADPGK, ADP-dependent glucokinase; ADPPFK, ADP-dependent phosphofructokinase; PDB, Protein Data Bank; mADPGK, mouse ADPGK; hADPGK, human ADPGK.

This is an Open Access article under the CC BY license.

liganded states are consistent with an induced fit ligand-binding model involving a hinged rigid body interdomain conformational change with a domain closing movement over the ADP and glucose once bound in the active site. Kinetic studies of *T. litoralis* ADPGK have led to a proposed ordered sequential enzymatic mechanism with MgADP binding before D-glucose (10). This mechanism has been rationalized with respect to the observed structural states, although SAXS data suggest that the conformational change in solution is greater than that seen by the ADPGK crystal structures (10). For archaeal ADPGKs, the specificity for ADP over ATP has been explained by amino acid side chains within the nucleotide binding site positioning the ADP β-phosphate in an homologous position to the γ-phosphate of ATP-dependent kinases (9) for phosphoryl transfer.

Because the function of eukaryotic ADPGK remains unclear, we have determined the structures of mammalian apo-ADPGK to 2.1 Å resolution and AMP-bound ADPGK to 3.0 Å resolution, shown substrate specificity for glucose, and investigated AMP and glucose inhibition. We show that mammalian ADPGK conserves the ribokinase-like fold of archaeal orthologues and highlight features of the enzyme active site, confirming the identity of key amino acids by site-directed mutagenesis. We have characterized AMP and glucose inhibition and shown that mammalian ADPGK has a strong preference for glucose with no activity with other sugars tested as substrate, including 2-deoxyglucose, the glucose analogue in widespread clinical use for detection of a variety of tumors by positron emission tomography (11).

Materials and Methods

Cloning of Recombinant Mammalian ADPGK—Sequence analysis predicted a possible N-terminal signal sequence for mammalian ADPGK (*e.g.* SignalP4.1 (12), mouse ADPGK (mADPGK) 1–18, and human ADPGK (hADPGK) 1–22, so a number of N-terminally truncated ADPGK cDNA sequences were designed, as well as full-length sequences. The cDNA for mADPGKΔ51 amino acids 52–495 and hADPGK (Δ50, Δ151, or full-length) codon-optimized for expression in *Escherichia coli* were PCR-subcloned into vector pBAD-TOPO, and the resulting vectors pBAD-mADPGKΔ51 and pBAD-hADPGK were sequence-verified. Mutant hADPGK constructs (D84A, R228A, H264A, H382A, H382V/H387V, H387A, D481A, D481E, and D481E) were prepared using whole plasmid PCR with primers containing the required nucleotide substitution with pBAD-hADPGK as template. The hADPGK numbering is +1 relative to mADPGK after amino acid 313. The presence of the mutated nucleotide substitution(s) was confirmed by DNA sequencing.

Purification of Mammalian ADPGK—For ADPGK expression *E. coli* LMG194 were transformed with the appropriate pBAD construct encoding hADPGK variants or mADPGKΔ51 and grown in 2× YT medium containing 100 μg/ml ampicillin. Cultures were grown at 37 °C to an A_{600} of 0.8 and induced with 0.1% (w/v) L-arabinose. The cells were harvested after 12 h by centrifugation for 20 min washed in cold PBS buffer and frozen at −80 °C. The cell pellets were resuspended in lysis buffer (50 mM Tris, pH 8.0, 500 mM NaCl, 4 mM DTT, Roche complete protease inhibitor tablet EDTA-free) and lysed by two passes through a French press. The soluble fraction was separated from cell debris by centrifugation at 46,000 × *g* for 90 min at 4 °C. Imidazole was added to the supernatant to a final concentration of 20 mM. The solution was loaded onto a 5-ml Ni^{2+}-NTA HisTrapFF column. ADPGK was eluted with a linear gradient from 20 to 500 mM imidazole in phosphate buffer (25 mM Na_2HPO_4, pH 8.0, 500 mM NaCl, 500 μM DTT, or 2 mM β-mercaptoethanol). The elution fractions containing ADPGK were pooled, dialyzed against low ionic strength binding buffer (40 mM Tris, pH 8.0, 20 mM NaCl), loaded onto a Uno Q6 column (Bio-Rad) pre-equilibrated with binding buffer, and eluted with a linear gradient to 1 M NaCl in Tris buffer, pH 8.0. The elution fractions containing ADPGK were pooled and concentrated, and glycerol was added to 20% (w/v) before storage at −20 °C (hADPGK) or directly frozen (mADPGK).

Analytical Gel Filtration Chromatography—Analytical gel filtration was used to estimate the oligomerization state of hADPGK on a Superdex 200 10/300 GL column (GE Healthcare) in 40 mM Tris buffer (pH 8.0), 200 mM NaCl. For column calibration blue dextran, alcohol dehydrogenase, bovine serum albumin, carbonic anhydrase, and cytochrome *c* were used as molecular weight standards in addition to previously characterized recombinant mADPGK. The purified human ADPGK for kinetic studies was shown to be in monomeric state in solution by analytical gel filtration, comparable to the mADPGK (2).

Mammalian ADPGK Crystal Structure Determination—Crystals were obtained from a mADPGKΔ51 solution of initial concentration 9.0 mg/ml (20 mM HEPES, 25 mM NaCl, 1 mM TCEP) after hanging drop vapor diffusion for 2 weeks with precipitant 0.2 M NH_4Cl, 20% (w/v) PEG 3350 (JCSG screen condition A9; Molecular Dimensions) at 21 °C. These crystallization conditions were refined with an additive screen. X-ray diffraction data were collected on a crystal grown in the above conditions supplemented with Silver Bullets Bio condition A1 (Hampton Research). For AMP crystal soaking experiments, larger mADPGKΔ51 single crystals were obtained by seeding. Crystallization drops were set up with 0.2 M NH_4Cl and 20% (w/v) PEG 3350 mixed with mADPGKΔ51 solution of initial concentration 9.0 mg/ml and incubated at room temperature for 2 weeks. Seeding was then performed placing small needle shaped crystals into an equilibrated drop of the same experiment where no nucleation event had occurred, and the crystals were incubated for another 2 weeks. AMP was introduced to select crystals by addition to a final concentration of 5 mM, and the experiment was incubated for another 4 days at room temperature, during which minimal cracking of the crystals was observed.

X-ray diffraction data of 0.5° oscillation images over a total scan range of 120° were collected on the MX2 beam line at the Australian synchrotron at 100 K from single crystals of apo-mADPGKΔ51 frozen in a loop by rapid immersion in liquid N_2 using perfluoropolyether oil as cryoprotectant. For the AMP-bound mADPGKΔ51, 0.5° oscillation images were collected on a Rigaku Micromax HF007 equipped with R-Axis IV detector at 120 K frozen in a loop with paratone N as cryoprotectant. Crystals were of orthorhombic symmetry with a solvent content of ~43% with one molecule in the asymmetric unit. Diffraction intensities were processed with XDS (13) and Pointless/Aim-

TABLE 1

X-ray diffraction data and refined ADPGK model statistics

$R_{merge} = \Sigma|I_i - <I_i>|/\Sigma I_i$ where I_i is the intensity of a single reflection, and $<I_i>$ is the mean intensity of that reflection. $r = \Sigma|F_o - F_c|/\Sigma F_o$. R_{free} is the R factor calculated for the cross-validated test set of reflections. Geometry scores and Ramanchandran statistics calculated with MolProbity (37). R_{merge}, R_{pim}, and $CC_{½}$ were calculated by Aimless as defined in Ref. 14.

	Apo-ADPGK	AMP-ADPGK
PDB code	5CCF	5CK7
Beam source	Australian Synchrotron MX2	Rigaku Micromax 007
Detector	Quantum 205	R-Axis IV
Distance to detector (mm)	315	200
Wavelength (Å)	0.9184	1.5418
Resolution range (Å)	47.42–2.09 (2.17–2.09)	30.00–2.99 (3.20–2.99)
Space group	$P2_12_12_1$	$P2_12_12_1$
Unit cell dimensions (Å)	45.92, 58.68, 160.94	45.68, 58.49, 161.71
Total number of reflections	126,165	53,669 (6,958)
Number of unique reflections	24,797 (1,318)	9,031 (1,438)
Multiplicity	4.8 (4.9)	5.9 (4.8)
Completeness (%)	99.5 (99.8)	97.1 (88.3)
Mean $I/\sigma I$	9.3 (2.0)	10.1 (2.8)
Wilson B factor (Å^2)	19.2	51.5
R_{merge}	0.12 (0.77)	0.091 (0.61)
R_{pim}	0.088 (0.43)	0.10 (0.37)
$CC_{½}$	0.98 (0.57)	0.99 (0.77)
R_{work} (%)	19.2 (29.3)	22.7 (32.6)
R_{free} (%)	24.2 (31.5)	24.3 (29.8)
Number of non-hydrogen atoms	3729	3497
Number of ligand molecules	0	1
Number of water molecules	282	27
Number of protein residues	446	447
Root mean square deviation bonds (Å)	0.009	0.015
Root mean square deviation angles (°)	1.27	1.69
Ramachandran favored (%)	98	97
Ramachandran outliers (%)	0.45	0.45
MolProbity score	0.61	2.11
MolProbity clash score	0.29	8.2
Average B factor (Å^2)	36.2	64.1

less (14) in the most likely space group $P2_12_12_1$ based on diffraction symmetry and systematic absences (Table 1). The apo-mADPGKΔ51 structure was solved by molecular replacement using Phaser (15) with a search model prepared in Phenix (16) from an ensemble of archaeal ADPGK large domain structures available from the PDB with model alteration (side chain and main chain deletions) informed by multiple sequence alignment. The molecular replacement solution was obtained with one molecule in the asymmetric unit, confirming the $P2_12_12_1$ space group, with positive difference density visible for the small domain and other atoms not included in the search ensemble. Extensive model rebuilding was carried out in Coot (17) in combination with auto-building and maximum-likelihood refinement conducted with Phenix (16) and Refmac (18) to build the small domain and improve the large domain structure. Solvent molecules were added to the model into positive 3 sigma peaks in the weighted $F_o - F_c$ difference map where chemically sensible hydrogen bonds could be made. The refinement (including TLS refinement) at later stages converged to yield a final model with an R factor of 0.192 and a free R factor of 0.242 (5% of reflections excluded from refinement) for data 47–2.10 Å. The AMP-mADPGKΔ51 structure was solved by molecular replacement in Phaser using the refined structure of apo-mADPGKΔ51 as a search model. The AMP-mADPGKΔ51 structure was refined, using restraints to the apo-mADPGKΔ51 structure, converging to an R factor of 0.227 and R_{free} of 0.243 (5% of reflections excluded from refinement) for data 39–3.0 Å. Further x-ray data and model quality statistics are presented in Table 1. The atomic coordinates and structure factor amplitudes for the apo-mADPGKΔ51 and AMP-mADPGKΔ51 crystal structures are available in the Research Collaboratory for Structural Bioinformatics Protein Data Bank under PDB codes 5CCF and 5CK7, respectively. The structure and sequence figures were prepared with CCP4mg (19) and Espript (20). Structural alignments were performed with Promals3D (21).

NMR Spectroscopy Assay for Mammalian ADPGK Substrate Specificity—For screening alternative hADPGK substrates with NMR spectroscopy, the following 1-ml reaction mixtures were set up: 100 mM KCl, 1 mM $MgCl_2$, 50 mM Bis-Tris-propane (pH 7.0 at 37 °C), 1 mM MgADP (first substrate) and 1 mM second substrate candidates. Tested candidates included D-glucose, L-glucose, 2-deoxyglucose, D-galactose, D-fructose, D-mannose, D-tagatose, L-rhamnose, D-glucosamine, D-xylose, D-ribose, *myo*-inositol, L-arabinose, D-arabinose, D-fructose-6-phosphate, α-D-glucose-1-phosphate, 1-*O*-methyl-α-D-glucopyranoside, 1-*O*-methyl-β-D-glucopyranoside, 3-*O*-methyl-D-glucopyranoside, and methyl-β-D-xylopyranoside. The reactions were started by the addition of hADPGK, and after incubation at 37 °C for 30 min, the reactions were stopped by adding 10 mM EDTA and heating to 80 °C for 5 min. For controls, the reaction mixtures were prepared without the addition of enzyme and/or MgADP. For NMR measurements, 5% D_2O was added for deuterium frequency lock to compensate for slight magnetic drifts of the NMR magnet. A Bruker Avance 400 MHz NMR spectrometer, operating at 400.13-MHz proton frequency, was used with a 5-mm QNP 1H/13C/31P/19F probehead. One-dimensional proton (^{1}H) spectra were acquired with presaturation or excitation sculpting to suppress the abundant water signal and 32,768 data points, 32 scans, 16.0204-ppm spectral width (6,410.256 Hz), and 2.0-s pulse delay time. One-dimensional phosphorus (^{31}P) spectra were acquired with and without power-gated decoupling with 65,536 data points, 2,048 scans,

400.9142-ppm spectral width (64,935.066 Hz), and 4.0 s delay time. Two-dimensional ^{31}P-^{1}H HMBC spectra were recorded with a pulse sequence that is optimized for long range couplings, with no decoupling during acquisition and using shaped pulses for off resonance presaturation. Parameters included: 4,096 × 64 data points, 16.0204 × 20.0013-ppm sweep width, 256 scans, and 3.0 s relaxation delay time. The spectra were processed with Topspin versions 1.3 and 2.1 (Bruker-Biospin, Rheinstetten, Germany). NMR assignments were confirmed by adding known amounts of ADP, AMP, and glucose-6-phosphate and repeating the NMR experiments.

ADPGK Kinetic Analysis—Human ADPGK enzymatic activity was measured in triplicate using a coupled assay with glucose-6-phosphate dehydrogenase as previously described (2, 3). Assays contained 50 mM Bis-Tris-propane (pH 7.0 at 37 °C), 100 mM KCl, 1 mM $NADP^+$, 1:1 molar ratio of ADP-$MgCl_2$, 2 units *Leuconostoc mesenteroides* glucose-6-phosphate dehydrogenase (Sigma-Aldrich). Units are defined as μmol/min. For ease of comparison of ADPGK activity to previously characterized hexokinases, assays were conducted at the "conventional" pH of 7.0. The glucose-6-phosphate dehydrogenase concentration was kept in large excess for all coupled assays. For measurement of the pH optimum of hADPGK activity the Bis-Tris-propane pH was varied from 6.0 to 9.25 in steps of 0.25. For determination of apparent K_m values for MgADP or D-glucose, the other substrate was kept constant; D-glucose 0.7 mM or MgADP 1 mM. Analysis of AMP product inhibition was assayed by adding increasing concentrations of AMP (0, 1, 2, 5, and 10 mM) to reactions containing 0.7 mM glucose and variable concentrations of ADP. The values for K_m and K_i were determined by nonlinear regression with Prism 6 (GraphPad Software). Inhibition by the product AMP was modeled to a kinetic model for competitive inhibition.

$$v = \frac{V_{max}[S]}{[S] + K_m\left(1 + \frac{[I]}{K_i}\right)} \quad \text{(Eq. 1)}$$

Inhibition by high concentrations of glucose substrate was modeled using the following equation.

$$v = \frac{V_{max}}{1 + \frac{K_m}{[S]} + \frac{[S]}{K_i}} \quad \text{(Eq. 2)}$$

The activities of site-directed mutant ADPGK enzymes were measured in the same assay format. Assays were carried out at least in duplicate in 100-μl microcuvettes using a Cary 300 UV-visible spectrometer. The detection level for null activity for mutant ADPGK is estimated at 1:100,000 of wild type ADPGK activity (3×10^{-4} units/mg).

Results

Structure of Mammalian ADPGK—The apo-mADPGKΔ51 (amino acids 52–495) crystal structure has been determined using x-ray diffraction data to 2.1 Å and refined to an *R* factor of 0.19 and a free *R* factor of 0.24. The asymmetric unit of the $P2_12_12_1$ cell contains a single ADPGK molecule consistent with a monomeric structure for ADPGK with no crystallographically related intermolecular contacts greater than 739 Å^2 as determined with PISA (22). Size exclusion chromatography during protein purification indicated a monomeric solution state (2).

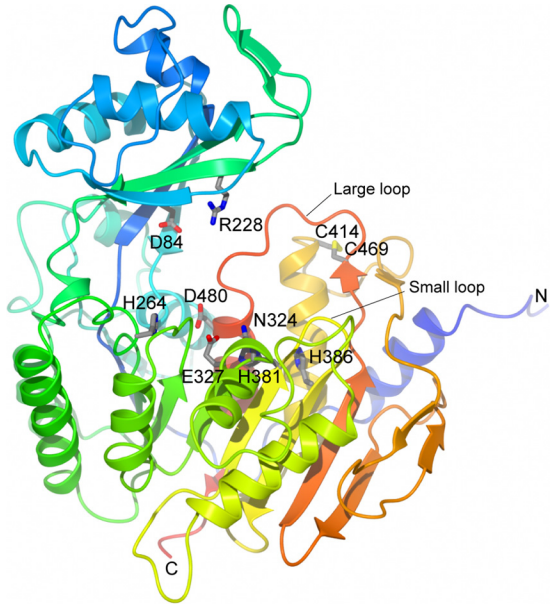

FIGURE 1. **The structure of mouse ADPGK.** Shown is a ribbon representation of the mADPGKΔ51 structure color-ramped *blue* to *red* from the N to C termini. The large (*orange*) and the small (*yellow*) nucleotide-binding loops are labeled. The disulfide bond is displayed as *sticks* with sulfurs in *yellow* (Cys-414–Cys-469), and other key amino acid side chains are displayed in stick representation colored by atom type.

The mammalian ADPGK structure has a ribokinase-like topology (Fig. 1) similar to that of other members of the PfKC (ADP-dependent kinase-like) group of the ribokinase superfamily. This overall fold is similar to the archaeal ADPGK and ADPPFK enzymes consisting of a large domain and a small domain connected by an intermediate hinge-containing region. Compared with archaeal ADPGK structures, the mADPGK structure is most similar to the unliganded "open" ADPGK conformation with a solvent-exposed active site cleft between the two domains (Fig. 1).

The large domain is comprised of a central curved 10-stranded mostly parallel β-sheet that packs against 5 helices on its convex face and 4 helices on its concave side. The small domain core comprises a curved 5-standed (β-strands 2–4, 8, and 11) β-sheet with 3 α-helices (2–4) and 2 additional short β-strands (9, 10) on the top of its convex face. The concave face of the sheet is unadorned and forms the upper part of the active site located between the two domains. Loops and three short helices form the complex multielement intermediate hinge region connecting the two domains.

The region most divergent from archaeal ADPGKs is after helix α14 (*i.e.* residue Cys-414) where α15 is much shorter and α16 is replaced in mADPGK (430–445) with a short two-stranded antiparallel β-sheet (Figs. 2 and 3) occupying a similar position and volume on the protein structure as the helices do for archaeal ADPGK. This change requires a minor reorientation of α1 at the N terminus. The structure of the mADPGK small lid domain compared with *P. furiosus* ADPGK (PDB code

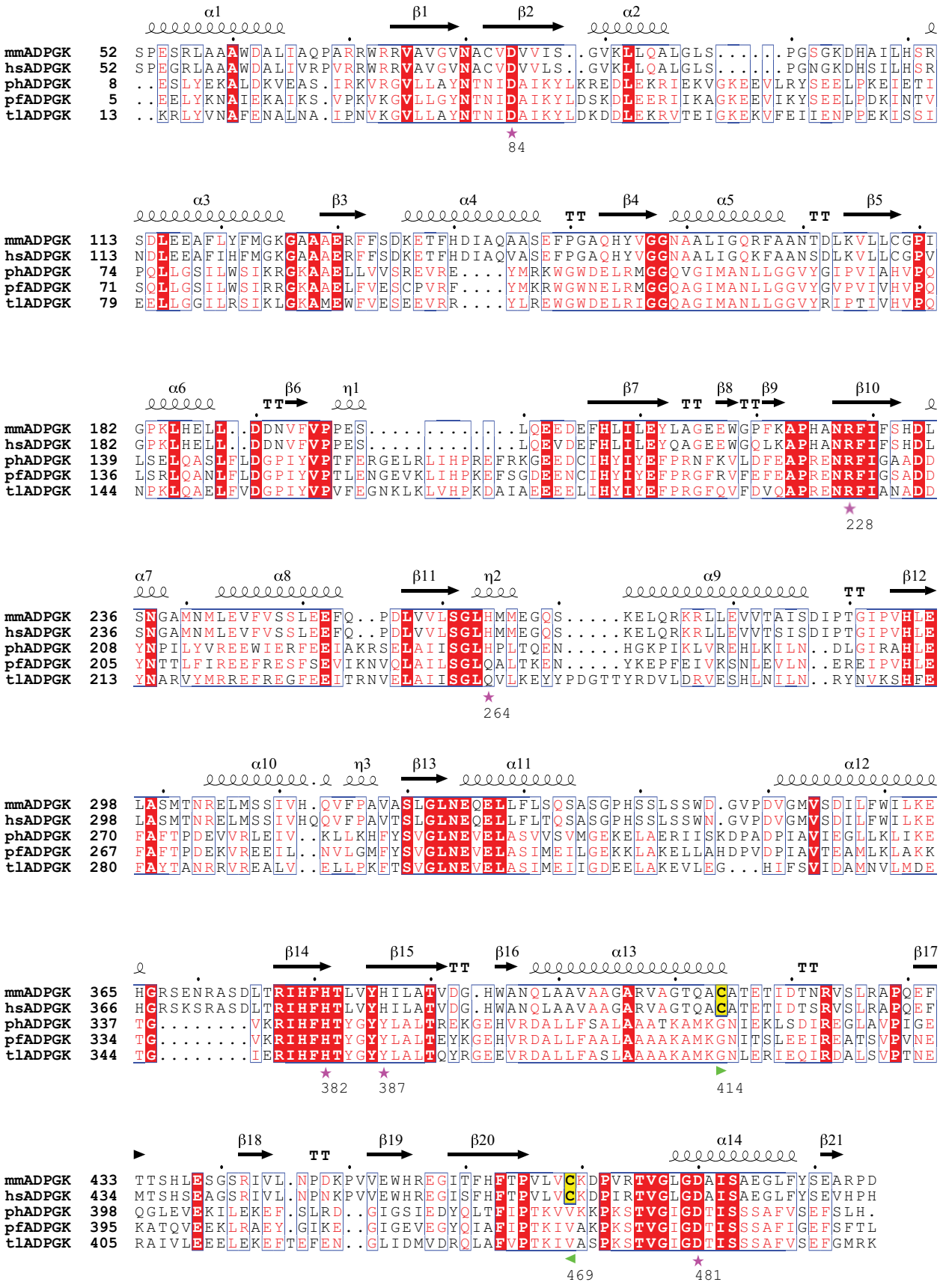

FIGURE 2. **ADPGK structure-based sequence alignment.** PromalS3D sequence alignment based on the structure of mouse ADPGK and the structures of archaeal ADPGKs. Helices (α, η), sheets (β), and turns (TT) in the structure of mADPGK are labeled. The mADPGK disulfide bond Cys are marked with *green triangles*. hADPGK residues targeted for site-directed mutagenesis are marked with *red stars*. *mm, M. musculus; hs, Homo sapiens; ph, P. horikoshii; pf, P. furiosus; tl, T. litoralis.*

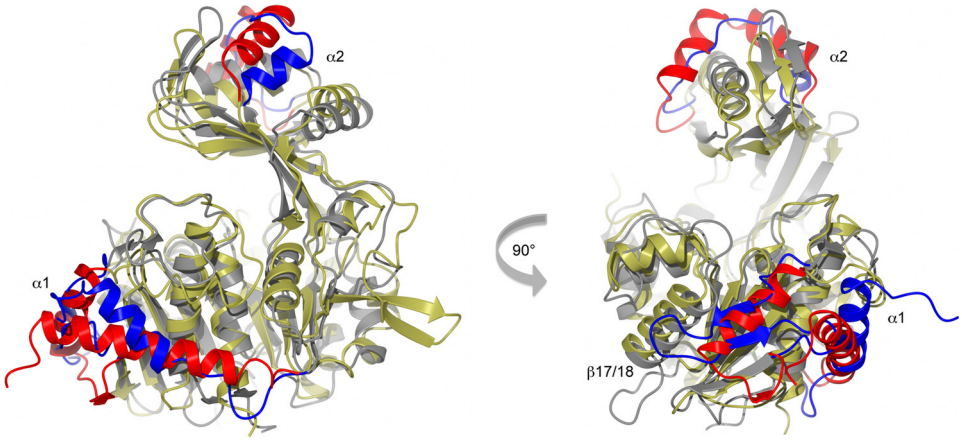

FIGURE 3. **Structural superposition of mouse and archaeal ADPGK structures.** The superposition of mADPGKΔ51 and *T. litoralis* ADPGK (PDB code 4B8R) in ribbon representation. Regions distinctly different from the archaeal ADPGK on the small (α2) and large (α1 and β17/18) are colored (*gray/blue* for mADPGK and *yellow/red* for *T. litoralis* ADPGK).

1L2L) shows a rearrangement of secondary structure elements; the structures of the α2 and α3 helices are not conserved for mADPGK with α2 shifted and α3 replaced by an extended β-strand region instead in mouse (Gly-97–Asp-105, helix α2; Fig. 3). The core of the small domain; the α4, α5 helices and β3-β4 strands are structurally conserved. Structural rigid body superposition using RAPIDO (23) allowing two domain structural alignment resulted in superposition of mADPGK with the closed *P. furiosus* ADPGK structure with an root mean square deviation 0.9 Å compared with 5.2 Å calculated with a single body superposition (359 Cα atoms used for superposition in both cases).

ADPGK Nucleotide Binding Site—Overall, the mADPGK structure contains homologous glucose and nucleotide binding sites compared with archaeal orthologues, although there are differences in the details of key residues lining the active site. The AMP-mADPGK structure reveals clear density for AMP reaction product bound in the nucleotide binding site (Fig. 4, *A* and *B*), whereas apo-mADPGK contains ordered solvent molecules in the active site. One striking feature of the mADPGK structure is the presence of a disulfide bond between Cys-469 at the "back" (relative to the ADP binding site) of the "large nucleotide-binding loop" (residues 466–476) that wraps around the ADP adenine and Cys-414 at the C terminus of α-helix 13 (Fig. 4*C*). Sequence alignments show these cysteine residues to be invariant among metazoan ADPGKs (Fig. 5), implying that the disulfide is a conserved feature for this phylogenetic group but not conserved for the archaeal enzymes. Archaeal ADPGKs have a similar backbone conformation in the absence of a disulfide bond with the structural requirements of the large nucleotide loop reinforced by hydrophobic contacts between the structurally orthologous amino acids, *i.e. P. furiosus* ADPGk Met-374–Val-429 (*T. litoralis* ADPGK Met-384–Val-440). Unliganded archaeal ADP sugar kinases, have a flexible large nucleotide-binding loop being either disordered in the absence of nucleotide (phADPGK) (7) or undergoing a conformational change upon nucleotide binding (ADPPFK) (24), inferring an induced fit for this loop upon nucleotide binding for archaeal enzymes. For ribokinases the large nucleotide (ATP) binding loop is structured by the binding of monovalent cations (25). The structure of the mADPGK large nucleotide loop, organized in part by the disulfide, facilitates nucleotide positioning and specificity for mADPGK. mADPGK contains the characteristic ribokinase family NEXE (residues 324–327) sequence motif proposed as binding Mg^{2+}. The AMP bound mADPGK structure shows Asn-324 and His-381 are positioned to interact with the nucleotide α-phosphate. The main chain NH of Leu-478–Gly-479 provide a helical N-terminal α-helix capping oxyanion site for electrostatic interaction with the nucleotide phosphate. The main chain at the N terminus of helix α14 476–482 rigid body shifts to accommodate the AMP, although overall tertiary changes upon nucleotide binding are minimal (Fig. 4*D*) The adenine $6NH_2$ and 1N interact with Cys-469 (of the disulfide bond) main chain carbonyl and NH groups, respectively. Leu-383, Ala-413, Val-468, and Leu-478 form hydrophobic contacts with the adenine. Asn-227 and Arg-228 are located on the small lid domain; if mADPGK undergoes a broadly similar domain closure to archaeal ADPGK (10), then these two residues would be positioned at the active site where they can contact nucleotide PO_4^{2-} (Fig. 1).

The sequence and structural differences between mammalian and archaeal ADPGKs are comparatively greater on the "small nucleotide-binding loop." For archaeal ADPGK, it has been proposed that a conserved Tyr (Tyr-357 for *T. litoralis* ADPGK and Tyr-347 for *P. furiosus* ADPGK) is responsible for the preference for ADP binding over ATP because its side chain excludes the larger triphosphate nucleotide and places the ADP into a binding mode where the β-phosphate is located in the equivalent γ-phosphate position found for ATP-dependent ribokinases (9). A homologous Tyr is not conserved for mammalian ADPGK and instead is His at the equivalent position. However, it has not been possible to convert an ADP-dependent enzyme to utilize ATP based on this hypothesis (hADPGK H382V/H387V; this study or Ref. 24). Furthermore, the mADPGK nucleotide-binding site appears more open partly because of replacement of another conserved archaeal ADPGK Tyr with Leu-383 at the C-terminal end of β14 (Fig. 2). The AMP ribose 2′ and 3′ OH contact the Thr-382 and His-381 main chain carbonyls and the His-381 side chain, respectively (Fig. 4), interactions conserved for archaeal ADPGK. The large nucleo-

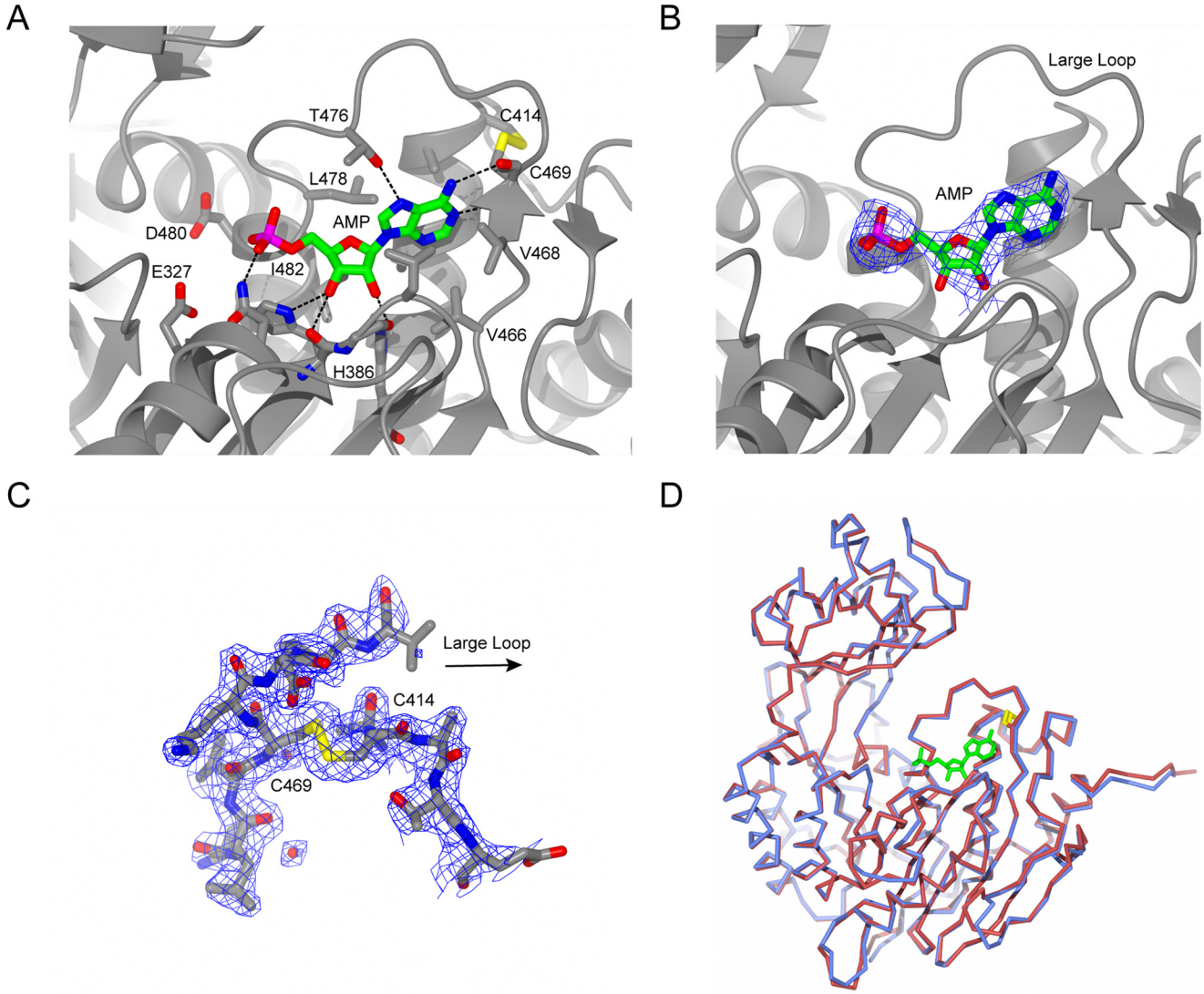

FIGURE 4. **Mouse ADPGK nucleotide binding.** *A*, the orientation and color coding of the structural representation are similar to Fig. 1. AMP and selected side chains are shown in stick representation color-coded by atom type. *B*, electron density around the AMP bound to ADPGK. The electron density is displayed as a *blue mesh* (contoured at 1.0 σ) and clipped to the AMP molecule. *C*, electron density defining the ADPGK disulfide bridge. The electron density is displayed as a *blue mesh* (contoured at 1.2 σ). *D*, backbone representation of the apo- (*blue*) and AMP-bound (*red*) mADPGK structures. The AMP and the disulfide bond are displayed in *green* and *yellow stick* representation, respectively.

tide binding loop (residues 466–476) and the strictly conserved Ile-482 (and to a lesser degree Leu-478) on either side of the catalytic Asp-480 (Fig. 2) are larger side chains compared with ribokinases (*e.g.* Ala-253 PDB code 1RK2) (26) that position the nucleotide along one "phosphate spacing" so that the ADPGK ADP β-phosphate is in an equivalent position to the γ-phosphate of ATP in ribokinase structures.

ADPGK Glucose Binding Site—Attempts to co-crystallize or soak mADPGK with glucose have not been successful to date; in the absence of a bound structure, it is possible to infer an homologous glucose binding site at the intermediate hinge region between the large and small domains for the mADPGK structure based on archaeal ADPGK (Fig. 6). The mADPGK structure shows that the GG (157–158) ribokinase sugar-binding sequence motif is conserved where the Gly-158 backbone NH can interact with glucose 4OH (by homology to archaeal ADPGK). mADPGK also contains the conserved glucose ligands from the lid domain Asp-84 (β2) and Glu-130 (β3). If we hypothesize a lid-closing mechanism equivalent to archaeal ADPGK occurring for mADPGK, then Asp-84 and Glu-130 would be positioned so that their side chains could make hydrogen bonds with the glucose 3 and 4OH, and 2OH, respectively. His-207 contacts with 2 and 3OH, further contributing to hexose specificity (8). One difference for mADPGK is Cys-82, which is Asn for archaeal ADPGKs (*e.g. P. furiosus* ADPGK Asn-32 and tlADPGK Asn-40) with the mADPGK sulfhydryl potentially in contact distance of the glucose 3OH. Another difference for mADPGK is the larger amino acids His-264–Met-265 compared with archaea *T. litoralis* ADPGK Gln-243–Ala-244 and *P. furiosus* ADPGK Gln-235–Val-236. The Met-265 side chain is positioned within 4 Å of the glucose-binding site, approaching the 2OH position. The catalytic Asp-480 is positioned within 3 Å of the glucose 6OH in this binding model. RAPIDO structural superposition of mADPGK with liganded archaeal ADPGK, allowing rigid body rotation of the two domains, positions conserved residues from the lid domain

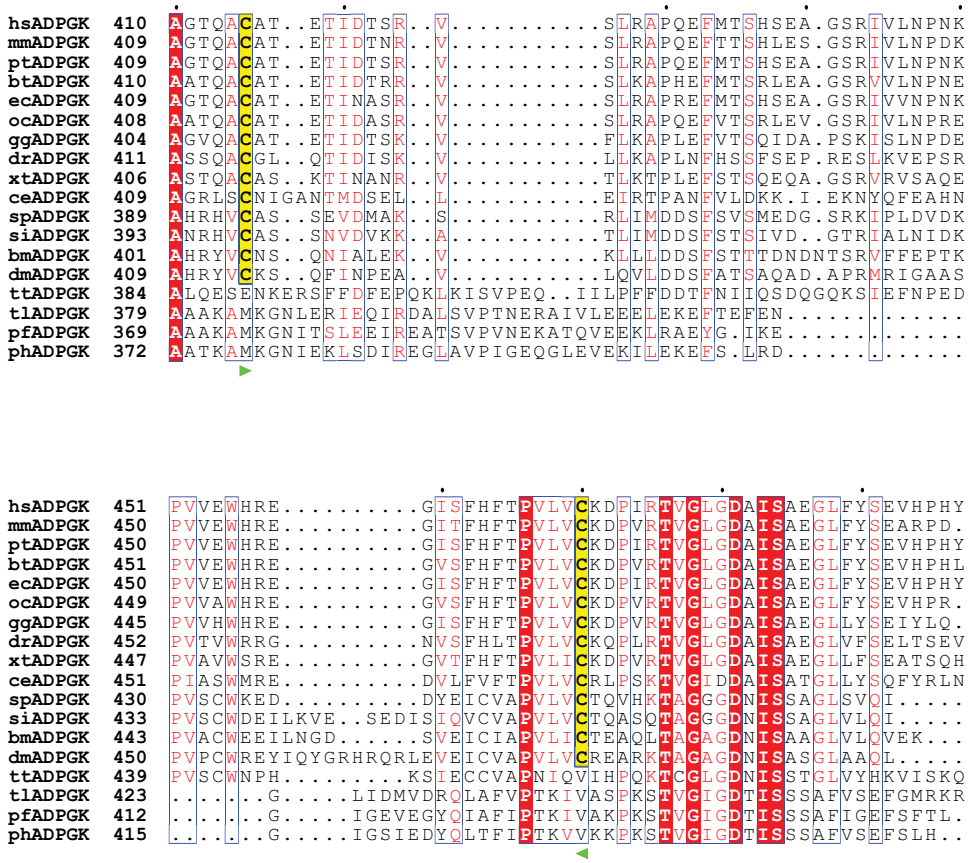

FIGURE 5. **Sequence alignment of the C-terminal region of ADPGKs from Eukaryotes and Archaea.** hs, *H. sapiens*; *mm*, *M. musculus*; *pt*, *Pan troglodytes*; *bt*, *Bos taurus*; *ec*, *Equus caballus*; *oc*, *Oryctolagus cuniculus*; *gg*, *Gallus gallus*; *dr*, *Danio rerio*; *xt*, *Xenopus tropicalis*; *ce*, *Caenorhabditis elegans*; *sp*, *Stronglycentrotus purpuratus*; *si*, *Solenopsis invicta*; *bm*, *Bombyx mori*; *dm*, *Drosophila melanogaster*; *tt*, *Tetrahymena thermophila*; *tl*, *T. litoralis*; *pf*, *P. furiosus*; *ph*, *P. horikoshii*. Cysteine residues homologous to those involved in the formation of the disulfide bond observed in *M. musculus* ADPGK are highlighted with *yellow shading*. The disulfide bond cysteines are indicated with a *green triangle*. The disulfide bond cysteines are highly conserved in Eukarya but absent in Archaea.

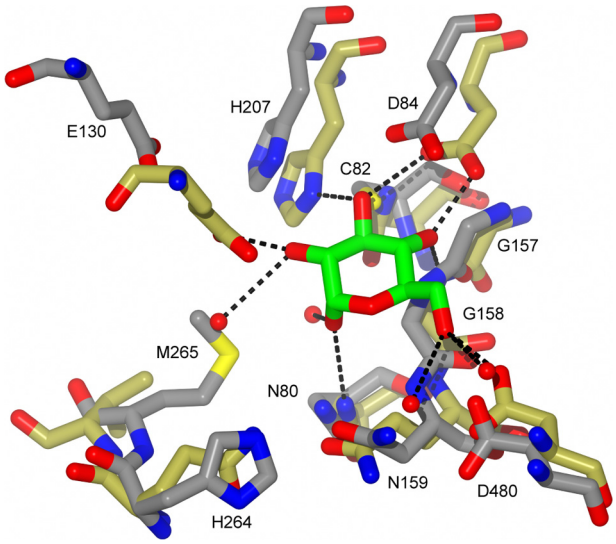

FIGURE 6. **Mouse ADPGK glucose binding site.** The mouse ADPGK glucose binding site inferred from homology to archaeal ADPGK by structural superposition of mADPGK (*gray*), and glucose/AMP bound *T. litoralis* ADPGK (PDB code 4B8S, *yellow*). The D-glucose (*green*) from 4B8S is displayed. All labels refer to mADPGK amino acids.

active site residues in close proximity to the glucose and ADP-binding sites, further highlighting the conservation with archaeal ADPGK.

ADPGK Functional Characterization—^{31}P NMR activity assays confirmed that D-glucose and ADP are substrates for human ADPGK. The assay monitored the disappearance of the substrate peak corresponding to ADP and appearance of signals for the products glucose-6-phosphate and AMP (Fig. 7). No activity was observed for any of the other sugars tested; 2-deoxyglucose, L-glucose, methyl-β-D-xylopyranoside, D-glucosamine, L-rhamnose, D-tagatose, 3-*O*-methyl-D-glucopyranoside, 1-*O*-methyl-β-D-glucopyranoside, 1-*O*-methyl-α-D-glucopyranoside, D-arabinose, L-arabinose, *myo*-inositol, D-ribose, D-xylose, D-galactose, D-fructose, D-mannose, D-fructose-6-phosphate, and α-D-glucose-1-phosphate.

The kinetic analysis for human ADPGK has been extended from previous studies (3) to include enzymatic parameters for ADP and to model the inhibition observed at higher glucose and ADP substrate concentrations, as well as AMP product inhibition. The pH profile for human ADPGK was determined with a single maximum activity at pH 7.5 in the range tested (pH 6.0–9.5). Allowing for inhibition at increased substrate concentrations in the kinetic model resulted in a V_{max} of 30 units/mg protein, an apparent K_m for glucose of 0.48 mM (±0.09) with an apparent K_i for glucose inhibition of 2.9 mM (±0.6) for hADPGK (Fig. 8). The apparent K_m for ADP was 0.56 mM (±0.09) with apparent substrate inhibition K_i of 9.1 mM (±1.5). The K_i for AMP inhibition was 0.5 mM (±0.07) (Fig. 8). hAD-

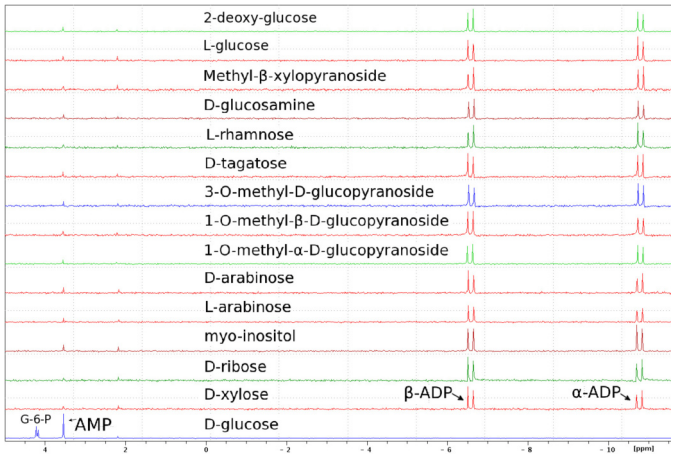

FIGURE 7. **^{31}P NMR spectra for screening substrate specificity of human ADPGK.** A control reaction with MgADP and D-glucose is shown at the *bottom*, where the signals for the products AMP and D-glucose-6-phosphate are indicated. No product was detectable for all other spectra and the signal intensity for the α- and β-anomers of ADP remained unchanged. *G-6-P*, glucose-6-phosphate.

PGK showed reduced activity with GDP (V_{max} 1.5 units/mg), relative to ADP, with an apparent K_m of 2.9 mM (±0.8). Little activity was observed for CDP, V_{max} 0.05 unit/mg. N-terminal truncations of human or mouse ADPGK (Δ50/Δ51, respectively) retained activity comparable with that of the full-length enzyme, but truncation of the N-terminal 151 amino acids (Δ151) abolished activity. Neither full-length nor N-terminally truncated ADPGK showed any observable activity with ATP. The hADPGK site-directed mutants showed either greatly reduced (D84A V_{max} 0.0004 unit/mg; R228A V_{max} 0.31 unit/mg, K_m = 0.27 mM for ADP and 0.23 mM for glucose; H264A V_{max} = 0.0051 unit/mg; D481A V_{max} = 0.15 unit/mg; D481N V_{max} = 0.017 unit/mg) or no detectable activity (H387A, D481E, and the double mutant H382V/H387V). Mutant hADPGK-H264A showed a greatly increased apparent K_m for glucose (5 mM), and no substrate inhibition could be detected for this variant with glucose concentrations of up to 55 mM.

Discussion

The overall fold of *Mus musculus* ADPGK is ribokinase-like, similar to archaeal orthologues although details differ in secondary structural elements of the lid domain and on the surface around the N terminus of the large domain. For crystallization the mouse ADPGK has been N-terminally truncated at residue 52 (Δ51) to the "core" ADPGK structure (conserved with archaea; Fig. 2). The very N terminus (residues 1–21) is predicted to be a signal sequence consistent with ER localization.

The mammalian ADPGK large nucleotide-binding loop is structured by a disulfide bond between two conserved cysteines; Cys-414 and Cys-469 for mADPGKΔ51 with the loop conformation retained in the absence of nucleotide. The only other ADPGK structure without a nucleotide bound is the *P. horikoshii* ADPGK (PDB code 1L2L), where the large nucleotide-binding loop is not defined in the electron density. Comparing the apo- and AMP-bound mADPGK structures shows that the large nucleotide binding loop is preformed in the absence of nucleotide. Mouse ADPGK was able to use GDP and CDP as phosphoryl donor with 55 and 12% relative (to ADP) activity remaining, respectively (2), compared with hADPGK with 5 and 0.2% activity with GDP and CDP, respectively. Human ADPGK showed no catalytic activity with UDP or TDP. In contrast, most archaeal ADPGKs, ADPPFKs, and ADPGK/PFKs can utilize nucleotide diphosphates other than ADP (27). For example, *P. furiosus* and *T. litoralis* ADPGK can use CDP at a similar rate to ADP, albeit with a much higher K_m (28), and lower catalytic rates were reported for the nucleotide diphosphates GDP, UDP, and IDP. On the other hand, no alternative nucleotide substrate utilization was observed for the *Archaeoglobus fulgidus* ADPGK (29). No ADP-dependent kinase has been identified that can use nucleotide triphosphate as phosphoryl donor, including the mutant hADPGK-H382V/H387V,

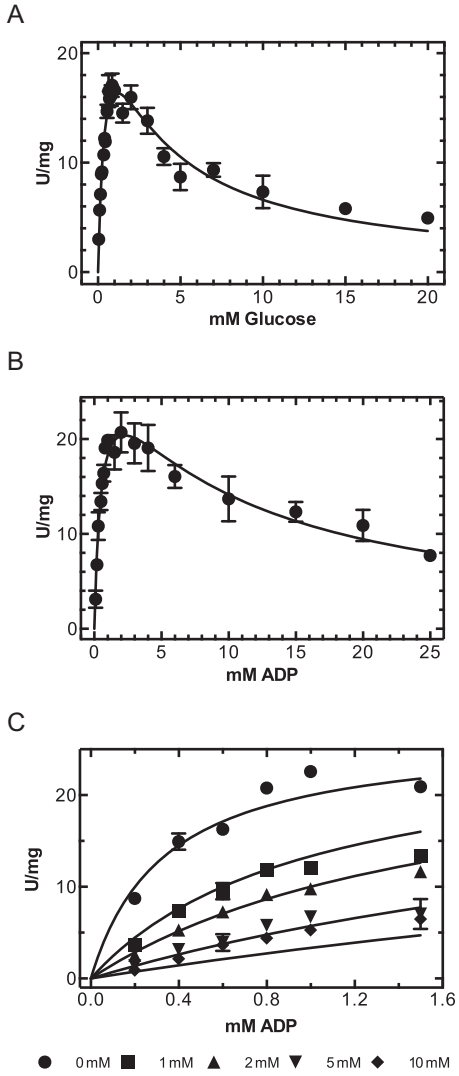

FIGURE 8. **Human ADPGK kinetic analysis.** *A*, the rate of enzymatic activity of hADPGK as a function of increasing concentration of D-glucose. Units (*U*) are defined as μmol/min. hADPGK showed inhibition at higher substrate concentrations, and the kinetic parameters were determined accordingly. The K_m and K_i for D-glucose were 0.48 mM and 2.9 mM, respectively. R^2 = 0.95. *Error bars* show standard deviation. *B*, the rate of enzymatic activity of hADPGK as a function of increasing concentration of MgADP. The K_m and K_i values for MgADP were 0.56 mM and 9.1 mM, respectively. R^2 = 0.96. *C*, enzyme kinetics of hADPGK, product inhibition by AMP as a function of increasing concentration of MgADP. AMP is a competitive inhibitor for MgADP binding to ADPGK with a K_i of 0.50 mM. The legend on the *right* shows the concentration of AMP. R^2 = 0.96. The kinetic parameters were determined by nonlinear regression with Prism 6.0.

which was designed with the aim of increasing active site volume to generate an ADPGK variant that could utilize ATP. An equivalent mutation in *P. furiosus* ADPPFK also did not result in a variant that could use ATP (24). The disulfide bond is consistent with the observed ER localization of mammalian ADPGK in tissue culture cell lines (4) and a predicted signal sequence. Sea urchin, various insects, and tetrahymena ADPGK (Fig. 6) contain an additional pair of cysteines that when aligned to the mADPGK structure are equivalent to residues Glu-453 and His-462 positioned adjacently across two β-strands (β19 and β20) at the appropriate distance to predict an additional disulfide in the ADPGK from these organisms.

It has been previously predicted that hADPGK residues 72–89 form an amphipathic helix proposed to be an ER membrane anchor (4). The mADPGK crystal structure shows this region to form two consecutive β-strands (β1 and β2) perpendicular to one another (with a bend in the middle around the *cis*-peptide at Gly-78) running from the large domain through the hinge region to the lid domain. This extended β-strand region forms part of the glucose-binding site with residues Cys-82 and Asp-84 lining the active site. It seems unlikely that this region would be membrane-inserted because it would require complete unfolding of the ADPGK structure to achieve this. The *cis*-peptide is present for *P. furiosus* ADPGK in which the Gly is conserved, but where Gly is substituted for Ala, *e.g. T. litoralis* ADPGK and *P. horikoshii* ADPGK, it is a *trans*-peptide. Based on the crystal structure, it is more likely than any membrane-inserted region of mADPGK region is N-terminal to residue 52, although no consensus membrane anchor regions are readily identified from the sequence other than the N-terminal signal sequence. The N-terminal ~50-amino acid region, not present in the mADPGK structure, is the most divergent region with respect to eukaryotic enzymes and is not present in archaeal ADPGK. There are two predicted N-terminal helices, one of which is proposed to be a cleavable signal peptide, although a role in membrane association anchoring cannot be ruled out by bioinformatic analysis alone, and then a Pro-Gly rich region. An interaction of human ADPGK with cholesterol has been identified (5); however, inspection of human and mouse ADPGK sequences reveals no unambiguous match to cholesterol binding consensus sequences such as the CRAC/CARC motifs, although other sequences can bind cholesterol (30).

hADPGK showed inhibition at biologically relevant glucose substrate concentrations, with activity reduced to ~50% at a concentration of 5.0 mM, suggesting that high D-glucose concentrations may exhibit a regulatory effect. The K_m value for ADP of hADPGK of 0.56 mM is within a comparable range to the mouse enzyme (2). Eukaryotic ADPGKs showed substrate inhibition for MgADP and product inhibition by AMP, although with relatively large K_i values relative to physiological nucleotide concentrations (31). The role of key catalytic residues was investigated by site-directed mutagenesis. Mutating the hADPGK catalytic Asp to D481A, D481N, or D481E reduced the relative activity to 0.5, 0.05, or 0%, respectively. An N-terminally truncated variant with the D481A mutation, hADPGKΔ50-D481A, was also inactive. The mutation R228A resulted in catalytic activity as low as 1% of the wild type enzyme with the apparent K_m values of 0.27 mM for ADP and 0.23 mM for glucose, which is still comparable the wild type enzyme. The R228A ADPGK is predicted to be unable to stabilize the terminal phosphate sufficiently during the reaction, whereas the substrate binding is affected to a lesser extent. A metal ion complexed with ADP is essential for ADPGK activity (32), although to date no definitive site for cation binding has been confirmed for any of the ADPGK crystal structures, as is the case for the mADPGK structures reported here. An exact role for the Mg^{2+} has not been elucidated, although for ribokinases, it has been hypothesized to stabilize transition state formation by increasing the electrophilicity of the phosphate for transfer (33).

Human ADPGK was found to be specific for D-glucose. The utilization of alternative phosphoryl acceptors was determined by monitoring ADP disappearance and AMP appearance by ^{31}P NMR, thus eliminating possible complications of a linked enzymatic assay, where the produced phosphorylated products may not be compatible with the linker enzymes. ADPGK from *T. litoralis* and *P. furiosus* had less than 10% of their activity with the hexoses galactose, fructose, or mannose (28, 34, 35). The archaeal enzymes were also able to utilize 2-deoxyglucose as phosphoryl acceptor to a certain extent. The *A. fulgidus* ADPGK was not able to use hexoses other than D-glucose and had low activity with 2-deoxyglucose (29). Human ADPGK, as for mADPGK shown previously (2), is not able to utilize 2-deoxyglucose as substrate. This was also this case for the mutant hADPGK-H264A, which was tested for different phosphoryl group acceptors because of its elevated K_m for glucose. The fact that eukaryotic ADPGK is apparently unable to accept a hexose phosphoryl acceptor modified in the 2-position has implications for probes used in positron emission tomography, an imaging technique widely in visualization of malignant tumor tissues that exploits the elevated glucose consumption of tumor cells. 2-^{18}F-fluoro-2-deoxy-D-glucose is frequently used for positron emission tomography imaging of tumors, which is metabolized after uptake into the cells by the hexokinases to 2-^{18}F-fluoro-2-deoxy-D-glucose-6-phosphate, which in turn cannot be further metabolized and is visualized by the positron emission tomography scanning technique (11, 36). A lack of ADPGK activity with 2-^{18}F-fluoro-2-deoxy-D-glucose could therefore lead to an underestimation of the total conversion of glucose to glucose-6-phosphate, which is an important metric in diagnosis.

Author Contributions—J. P. R., A. K. G., R. S. R., and A. J. S. S. conceived the study, performed the experiments and the subsequent analysis, and wrote the paper.

Acknowledgments—We thank Susan Richter, Kathryn Stowell, and William Wilson for much valuable discussion and Vince Carbone and Tom Caradoc-Davies for data collection at the Australian Synchrotron.

References

1. Kengen, S. W., de Bok, F. A., van Loo, N. D., Dijkema, C., Stams, A. J., and de Vos, W. M. (1994) Evidence for the operation of a novel Embden-Meyerhof pathway that involves ADP-dependent kinases during sugar fermentation by *Pyrococcus furiosus*. *J. Biol. Chem.* **269,** 17537–17541

2. Ronimus, R. S., and Morgan, H. W. (2004) Cloning and biochemical characterization of a novel mouse ADP-dependent glucokinase. *Biochem. Biophys. Res. Commun.* **315,** 652–658
3. Richter, S., Richter, J. P., Mehta, S. Y., Gribble, A. M., Sutherland-Smith, A. J., Stowell, K. M., Print, C. G., Ronimus, R. S., and Wilson, W. R. (2012) Expression and role in glycolysis of human ADP-dependent glucokinase. *Mol. Cell. Biochem.* **364,** 131–145
4. Kamiński, M. M., Sauer, S. W., Kamiński, M., Opp, S., Ruppert, T., Grigaravičius, P., Grudnik, P., Gröne, H.-J., Krammer, P. H., and Gülow, K. (2012) T cell activation is driven by an ADP-dependent glucokinase linking enhanced glycolysis with mitochondrial reactive oxygen species generation. *Cell Reports* **2,** 1300–1315
5. Hulce, J. J., Cognetta, A. B., Niphakis, M. J., Tully, S. E., and Cravatt, B. F. (2013) Proteome-wide mapping of cholesterol-interacting proteins in mammalian cells. *Nat. Methods* **10,** 259–264
6. Richter, S., Morrison, S., Connor, T., Su, J., Print, C. G., Ronimus, R. S., McGee, S. L., and Wilson, W. R. (2013) Zinc finger nuclease mediated knockout of ADP-dependent glucokinase in cancer cell lines: effects on cell survival and mitochondrial oxidative metabolism. *PLoS One* **8,** e65267
7. Tsuge, H., Sakuraba, H., Kobe, T., Kujime, A., Katunuma, N., and Ohshima, T. (2002) Crystal structure of the ADP-dependent glucokinase from *Pyrococcus horikoshii* at 2.0-Å resolution: a large conformational change in ADP-dependent glucokinase. *Protein Sci.* **11,** 2456–2463
8. Ito, S., Fushinobu, S., Jeong, J.-J., Yoshioka, I., Koga, S., Shoun, H., and Wakagi, T. (2003) Crystal structure of an ADP-dependent glucokinase from *Pyrococcus furiosus*: implications for a sugar-induced conformational change in ADP-dependent kinase. *J. Mol. Biol.* **331,** 871–883
9. Ito, S., Fushinobu, S., Yoshioka, I., Koga, S., Matsuzawa, H., and Wakagi, T. (2001) Structural basis for the ADP-specificity of a novel glucokinase from a hyperthermophilic archaeon. *Structure* **9,** 205–214
10. Rivas-Pardo, J. A., Herrera-Morande, A., Castro-Fernandez, V., Fernandez, F. J., Vega, M. C., and Guixé, V. (2013) Crystal structure, SAXS and kinetic mechanism of hyperthermophilic ADP-dependent glucokinase from *Thermococcus litoralis* reveal a conserved mechanism for catalysis. *PLoS One* **8,** e66687
11. Zhu, L., Ploessl, K., and Kung, H. F. (2013) Chemistry: expanding the scope of fluorine tags for PET imaging. *Science* **342,** 429–430
12. Petersen, T. N., Brunak, S., von Heijne, G., and Nielsen, H. (2011) SignalP 4.0: discriminating signal peptides from transmembrane regions. *Nat. Methods* **8,** 785–786
13. Kabsch, W. (2010) XDS. XDS. *Acta Crystallogr. D Biol. Crystallogr.* **66,** 125–132
14. Evans, P. R., and Murshudov, G. N. (2013) How good are my data and what is the resolution? *Acta Crystallogr. D Biol. Crystallogr.* **69,** 1204–1214
15. McCoy, A. J. (2007) Solving structures of protein complexes by molecular replacement with Phaser. *Acta Crystallogr. D Biol. Crystallogr.* **63,** 32–41
16. Adams, P. D., Grosse-Kunstleve, R. W., Hung, L. W., Ioerger, T. R., McCoy, A. J., Moriarty, N. W., Read, R. J., Sacchettini, J. C., Sauter, N. K., and Terwilliger, T. C. (2002) PHENIX: building new software for automated crystallographic structure determination. *Acta Crystallogr. D Biol. Crystallogr.* **58,** 1948–1954
17. Emsley, P., and Cowtan, K. (2004) Coot: model-building tools for molecular graphics. *Acta Crystallogr. D Biol. Crystallogr.* **60,** 2126–2132
18. Murshudov, G. N., Skubák, P., Lebedev, A. A., Pannu, N. S., Steiner, R. A., Nicholls, R. A., Winn, M. D., Long, F., and Vagin, A. A. (2011) REFMAC5 for the refinement of macromolecular crystal structures. *Acta Crystallogr. D Biol. Crystallogr.* **67,** 355–367
19. McNicholas, S., Potterton, E., Wilson, K. S., and Noble, M. E. (2011) Presenting your structures: the CCP4mg molecular-graphics software. *Acta Crystallogr. D Biol. Crystallogr.* **67,** 386–394
20. Gouet, P., Courcelle, E., Stuart, D. I., and Metoz, F. (1999) ESPript: analysis of multiple sequence alignments in PostScript. *Bioinformatics* **15,** 305–308
21. Pei, J., Kim, B. H., and Grishin, N. V. (2008) PROMALS3D: a tool for multiple protein sequence and structure alignments. *Nucleic Acids Res.* **36,** 2295–2300
22. Krissinel, E., and Henrick, K. (2007) Inference of macromolecular assemblies from crystalline state. *J. Mol. Biol.* **372,** 774–797
23. Mosca, R., Brannetti, B., and Schneider, T. R. (2008) Alignment of protein structures in the presence of domain motions. *BMC Bioinformatics* **9,** 352
24. Currie, M. A., Merino, F., Skarina, T., Wong, A. H., Singer, A., Brown, G., Savchenko, A., Caniuguir, A., Guixé, V., Yakunin, A. F., and Jia, Z. (2009) ADP-dependent 6-phosphofructokinase from *Pyrococcus horikoshii* OT3: structure determination and biochemical characterization of PH1645. *J. Biol. Chem.* **284,** 22664–22671
25. Li, J., Wang, C., Wu, Y., Wu, M., Wang, L., Wang, Y., and Zang, J. (2012) Crystal structure of Sa239 reveals the structural basis for the activation of ribokinase by monovalent cations. *J. Struct. Biol.* **177,** 578–582
26. Sigrell, J. A., Cameron, A. D., Jones, T. A., and Mowbray, S. L. (1998) Structure of *Escherichia coli* ribokinase in complex with ribose and dinucleotide determined to 1.8 Å resolution: insights into a new family of kinase structures. *Structure* **6,** 183–193
27. Merino, F., and Guixé, V. (2011) On the specialization history of the ADP-dependent sugar kinase family. In *Gene Duplication* (Friedberg, F., ed) pp. 237–256, Intech, Croatia
28. Koga, S., Yoshioka, I., Sakuraba, H., Takahashi, M., Sakasegawa, S., Shimizu, S., and Ohshima, T. (2000) Biochemical characterization, cloning, and sequencing of ADP-dependent (AMP-forming) glucokinase from two hyperthermophilic archaea, *Pyrococcus furiosus* and *Thermococcus litoralis*. *J. Biochem.* **128,** 1079–1085
29. Labes, A., and Schönheit, P. (2003) ADP-dependent glucokinase from the hyperthermophilic sulfate-reducing archaeon *Archaeoglobus fulgidus* strain 7324. *Arch. Microbiol.* **180,** 69–75
30. Fantini, J., and Barrantes, F. J. (2013) How cholesterol interacts with membrane proteins: an exploration of cholesterol-binding sites including CRAC, CARC, and tilted domains. *Front. Physiol.* **4,** 31
31. Veech, R. L., Lawson, J. W., Cornell, N. W., and Krebs, H. A. (1979) Cytosolic phosphorylation potential. *J. Biol. Chem.* **254,** 6538–6547
32. Merino, F., Rivas-Pardo, J. A., Caniuguir, A., García, I., and Guixé, V. (2012) Catalytic and regulatory roles of divalent metal cations on the phosphoryl-transfer mechanism of ADP-dependent sugar kinases from hyperthermophilic archaea. *Biochimie* **94,** 516–524
33. Matte, A., Tari, L. W., and Delbaere, L. T. (1998) How do kinases transfer phosphoryl groups? *Structure* **6,** 413–419
34. Verhees, C. H., Koot, D. G., Ettema, T. J., Dijkema, C., de Vos, W. M., and van der Oost, J. (2002) Biochemical adaptations of two sugar kinases from the hyperthermophilic archaeon *Pyrococcus furiosus*. *Biochem. J.* **366,** 121–127
35. Guixé, V., and Merino, F. (2009) The ADP-dependent sugar kinase family: kinetic and evolutionary aspects. *IUBMB Life* **61,** 753–761
36. Oriuchi, N., Higuchi, T., Ishikita, T., Miyakubo, M., Hanaoka, H., Iida, Y., and Endo, K. (2006) Present role and future prospects of positron emission tomography in clinical oncology. *Cancer Sci.* **97,** 1291–1297
37. Davis, I. W., Leaver-Fay, A., Chen, V. B., Block, J. N., Kapral, G. J., Wang, X., Murray, L. W., Arendall, W. B., 3rd, Snoeyink, J., Richardson, J. S., and Richardson, D. C. (2007) MolProbity: all-atom contacts and structure validation for proteins and nucleic acids. *Nucleic Acids Res.* **35,** W375–W383